A new platform for the determination of air-sea fluxes (OCARINA): Overview and first results

Denis Bourras, Hubert Branger, Gilles Reverdin, Louis Marié, Rémi Cambra, Lucio Baggio, Christophe Caudoux, Gérard Caudal, Simon Morisset, Nicolas Geyskens, et al.

A New Platform for the Determination of Air-Sea Fluxes (OCARINA): Overview and First Results

D. Bourras[1,], H. Branger[2], G. Reverdin[3], L. Marié[4], R. Cambra[1], L. Baggio[1], C. Caudoux[1], G. Caudal[1,], S. Morisset[3], N. Geyskens[5], A. Weill[1], and D. Hauser[1]

4 February 2014

Manuscript accepted for publication in the Journal of Oceanic and Atmospheric Technology

Corresponding author Email: denis.bourras@latmos.ipsl.fr

1 Université Versailles St-Quentin ; Sorbonne Universités, UPMC Univ. Paris 06 ; CNRS/INSU ; LATMOS-IPSL, 11 Bd d'Alembert 78280 Guyancourt
2 Aix Marseille Université ; CNRS ; Centrale Marseille ; IRPHE UMR 7342, F-13384, Marseille, France
3 Sorbonne Universités, UPMC Univ. Paris 06 ; CNRS/INSU ; LOCEAN, 1 place Jussieu 75252 Paris cedex 05
4 Ifremer-LPO, Technopôle de Brest - Pointe du Diable - 29280 Plouzané
5 CNRS, DT-INSU, 1 place Aristide Briand, 92195, Meudon Cedex

Abstract
The present paper describes a new type of floating platform that was specifically designed for estimating air-sea fluxes, investigating turbulence characteristics in the atmospheric surface boundary layer, and studying wind-wave interactions. With its design, it can be deployed in the open ocean or in shallow water areas. The system is designed to be used from a research vessel. It can operate for ~10 hours as a drifting wave rider and three hours under power. Turbulence and meteorological instrument packages are placed at a low altitude (1-1.5 m). It was deployed for validation purposes during the FROMVAR 2011 experiment off the west coast of Brittany (France). Wind friction velocity and surface turbulent buoyancy flux were estimated using eddy-covariance, spectral, bulk and profile methods. The comparisons of the four methods show a reasonable agreement except for the spectral buoyancy flux. This suggests that the platform design is correct. Also the wind measured at a fixed height above the sea shows spectral coherence with wave heights, such that wind and swell are in phase, with largest wind values on top of swell crests. This result in qualitative agreement with current model predictions supports the capability of OCARINA to investigate wind-swell interactions.

1. Introduction

Air-sea fluxes of momentum and heat, atmospheric turbulence in the surface atmospheric boundary layer, and wind-wave interactions are key characteristics that are needed to validate and improve dynamical models of the atmosphere, the upper ocean and waves.

There remains a need to better parameterize the flux-drag relation as a function of sea state (e.g. Donelan et al., 1993, Donelan et al., 1997), the determination of the so-called wind input function (e.g. Donelan, et al., 2005), and to improve the Kolmogorov (1941) and Monin-Obukhov (1954) theories in stable boundary layers (e.g. Weill et al., 2003) or in the presence of swell (Smedman et al., 2009).

There are three main methods for estimating air-sea turbulent fluxes, namely the Eddy Covariance method (hereafter referred as EC method, e.g. Katsaros et al., 1993, Anctil et al., 1994, Edson et al., 1998), the spectral method or Inertial-Dissipation method (ID method hereafter, Edson et al., 1991), and the similarity or bulk method (e.g. Liu et al., 1979, Fairall et al., 2003).

An experimental determination of air-sea turbulent exchanges has to fulfil four different requirements: (1) Using reliable and accurate instruments and recording a complete set of variables, (2) using a measurement platform that has the least possible impact on the quality of measurement data, (3) using instruments as close as possible to the sea surface, i.e not too far from the mean water level, and (4) having a correct operating strategy. Although these rules are purely technical and operational, they can affect substantially the overall quality of collected data. Therefore, it is necessary to optimize not only the measurement instruments, but also the measurement strategy and the platforms themselves.

The second, third and fourth requirements are strongly conditioned by the platform used, which until now has been either a fixed platform, a towed platform (e.g. Edson et al., 1998), a research ship (e.g. Katsaros et al., 1993, Christensen et al., 2013), a floating platform, or a buoy (Anctil et al., 1994, Weller et al., 2012, Graber et al., 2000). Hereafter, we attempt to briefly review the advantages and limitations of these platforms.

Fixed platforms such as the Woods Hole Oceanographic Institution (WHOI) Martha's Vineyards platform (Edson et al., 2007), or the Black Sea platform (e.g. Soloviev and Kudryavtsev, 2010) produce continuous sampling at the same location for several days to several years, which is of invaluable interest for the study of air-sea interactions. However, possible limitations are aerodynamic distortion, which largely depends on wind direction, and the fact that most of them are not in open sea conditions, in which case the results found with fixed platforms might be specific to the conditions associated with their geographic location.

Towed platforms, the use of which was pioneered by Katsaros et al (1980), are helpful for sampling small scale variations of the Sea Surface Temperature (SST) and of the Sea Surface Salinity (SSS), for example. However, they have limitations for wave, downwelling radiation and atmospheric turbulence measurements, because the apparatus naturally places itself in the disturbed atmospheric wake or in the bow wave of the ship. The proximity of the ship might affect radiation data because of its colour and its thermal radiation.

Quality air-sea flux data can be collected in the open ocean with a research vessel (R/V hereafter) or a floating platform such as the Floating Instrument Platform (FLIP, e.g. Millet et al., 2007). Unfortunately, such platforms are difficult to operate and ship cruises are expensive thus non-frequent. In spite of this, the use of R/Vs is by far the most convenient way to document flux variations in a large area, because R/Vs can cruise for up to several months. The main limitation of R/Vs is that they are affected by aerodynamic distortion of bulk quantities, but probably also at turbulent scales (Bourras et al., 2009). Note that data may also be affected by thermal effects (Berry et al., 2004). The aerodynamic distortion effect may have a large impact on the accuracy of flux estimates, because wind data are affected as a function of the shape of the ship, the location of the instruments on the ship, and the angle between the ship and the relative wind (Yelland et al., 2002). In addition, due to their large weight and dimension, most R/Vs have a large spectral motion peak in the same frequency range as waves and turbulence production (0.01-1 Hz), which is problematic for applying the EC method for example. Other issues include the height of measurement that may be considered as too far from the air-sea interface (+7 m to +17 m and -3 m for SST), or the position of the instruments that are located at the bow of the R/V, i.e. far from the centre of gravity of the R/V. As a result, the measurement height varies and the vertical wind component is disturbed. Associated with measurements on R/Vs is the issue of the displacement height, which may be difficult to assess (e.g. Brut et al., 2005, Popinet, Smith, and Stevens, 2004).

Buoys appear to be a good compromise for producing quality air-sea data, although an obvious limitation of buoys is that a ship is required for deployment, recovery, and maintenance, which is again a major operation. In addition, for buoys that are held in place for a long time (more than one month), instruments are more vulnerable to water, salt (corrosion or deposit on sensors) and fouling. To date, the Rosenstiel School of Marine and Atmospheric Science (RSMAS) Air-Sea Interaction Spar buoy (ASIS) is possibly the best attempt at buoy development dedicated to the study of air-sea interactions (Graber et al., 2000). It was recently proven to be successful even in severe weather conditions (Sahlée et al., 2012). Note that in very strong winds buoys can tilt relative to the vertical (Howden et al., 2008). Measuring fluxes must be very difficult in such conditions with any platform. The ASIS buoy presumably has small aerodynamic distortion and can be equipped with various instruments, which include not only turbulence, but also radiation, gas fluxes, and underwater instruments, thanks to its large payload capacity. Although there are few limitations associated with this design, it can be argued that it is rather heavy and large, which may limit the number of deployments. In addition, by its design, ASIS turbulence measurements are made at 3.5-4.5m above the surface, whereas the study of turbulence even closer to the surface may be of interest (Grare et al., 2013). Instruments are not at a constant height above the surface. The pertinence of this argument may be discussed. However, for the study of wave to wave wind variation, constant height wind data may be of interest.

In order to overcome the above limitations in designing a new platform, the five following desirable criteria were taken into consideration:

(1) Height above the sea surface should be constant, for analyzing wind-wave interaction.

(2) Flow distortion, thermal effects, and effect of the platform on waves would have to be small.
(3) Wind, temperature, and humidity measurements would be taken at heights smaller than existing designs (< 3m), and possibly at several heights, for investigating surface boundary layer profiles.
(4) Data would be sampled far from the host ship, to avoid the effects of host ship wake and radiation.
(5) Deployment and recovery would be as easy as possible, in order to insure instrument check, cleaning, maintenance, and for maximizing data return.

We propose a new platform design following these criteria: OCARINA, which stands for "Ocean Coupled to Atmosphere, Research at the Interface with a Novel Autonomous platform". It is described in section two. In section three, we briefly describe the environmental conditions of the experiment during which OCARINA was recently tested. Next in section four, its main features including flow distortion and motion characteristics are discussed. In section five, different estimates of air-sea fluxes done by this platform are compared and the wind stress angle is analysed with respect to the mean wind direction. In section six, eight cases of wind-wave interaction for which swell and wind travel in the same direction and in opposite direction are presented, respectively to further check the quality of the wind measurements in presence of swell. Lastly, the results are summarized and discussed in section seven.

2. Description of the platform

a. The platform

The OCARINA platform is a two-meter long trimaran boat that weighs ~35 kg (Figures 1,2). It has a streamlined shape and a low profile. As such, OCARINA has small aerodynamic distortion whatever the direction of the incoming wind is, see section 4a. OCARINA is motorized with a propeller coupled to an autopilot and a remote control. It can be controlled to follow a particular route, drift as a wave rider, or maintain its position, within the limit of its battery life, which is currently three hours at low speed (1.5 kts). Two independent 5 000 mAh Lithium-Polymer batteries of five 4.2 Volts cells each provide power for navigation, communication, science instruments and data storage, for up to twelve hours.

The trimaran configuration was chosen because it reduces self-roll as opposed to monohull designs. Another advantage of the configuration is that the whole payload can be installed on the central float. A catamaran is easier to construct, but the payload has to be split between the two hulls, or it has to be installed in a bulky compartment between the two side hulls.

Weight was kept as small as possible to facilitate transport and deployment. But above all, weight is a key point that conditions structure motion, together with the position of the instrument that measures turbulent wind and temperature fluctuations, presently located at the top of a central mast (so-called 'turbulent mast' hereafter) on OCARINA, as can be seen on Figures 1,2. On OCARINA, the small weight coupled with a turbulent mast at the centre of the ship induces minimal vertical motion relative to the surface (the platform does not dive or bounce on the surface). Note however that OCARINA presents the characteristic motion of

trimarans, which consists of a small precession-like motion, i.e. it rotates in circles between its two lateral hulls.

One particular feature that results from its small weight and its large projected horizontal surface is that the trimaran naturally follows the waves. Thus, to some extent (wavelengths larger than four meters), it is possible to deduce wave features just from the recorded motion/ inertial package.

The small size of OCARINA was well appreciated whilst carrying it on almost every type of host boat. It even held on the rear deck of a 7 m-long inflatable boat. Thus, it was easily accepted on science experiments, which helps for missions planned at short notice, for example.
Overheating of electronic and mechanical components inside the main float was avoided by choosing an electric engine located in an underwater bulb.

b. Science payload
The science instruments are installed at five different locations on OCARINA, as illustrated on Figures 1,2. There are three masts for atmosphere and radiation measurements, one Seabird SBE-37 on the side of the main hull for SST and SSS measurements, and one inertial platform at the horizontal centre of OCARINA and at the level of the waterline. The inertial platform is a Xsens MTI-G device that features three magnetometers, three accelerometers, three gyroscopes, a GPS and a barometer. The MTI-G is light, weighs 70 g, and is small. Motion data are recorded at 50 Hz. The turbulent mast holds a Gill Co. R3-50 sonic anemometer, at 1.5 m above the surface. It samples the three wind components as well as sound speed (which is related to the virtual temperature of the air), at the rate of 50 Hz. The port mast holds a Vaïsala WXT-520 meteorological station that measures air temperature and humidity, static pressure, rain, and wind, at 1 Hz. The station is located 1 m above the surface. This characteristic will be further discussed in section 7. Lastly, the starboard mast holds a Kipp & Zonen CNR-4 radiation instrument, which measures upward and downward radiation fluxes in the visible and infrared spectra. Overall, OCARINA samples and records over fifty variables simultaneously. The instruments and sampled variables are summarized in Table 1.

c. Data acquisition, automatic pilot and transmission
A specific Field Programmable Gate Array (FPGA) based electronic board was designed for data acquisition. It provides a lightweight, low consumption and above all a reliable method for sampling, sorting and adding time and date independently for all data. After experiencing data synchronization problems from various serial ports in past experiments, we decided to proceed with an asynchronous data processing on board. Every datum has its own time tag. Next, data are put in a heap memory and then stored and duplicated into two memory cards (SD cards) for robustness of the system, as represented on Figure 3. Time is inferred from an internal clock that is periodically synchronized to a GPS clock signal. This system was tested and verified: the time deviation was never larger than 0.01 ms, which is small compared to the sampling period of the instruments, i.e. 20 ms.

OCARINA has currently four operation modes. The first mode is a manual mode, which means that OCARINA is remotely controlled by an operator. This mode is helpful for

deploying and recovering OCARINA from the host ship in minutes. The second mode is called 'waypoint navigation': OCARINA follows a list of programmed waypoints, and cruises from one waypoint to the next. This mode can be used for surveys, or to test the impact of wind or wave orientation with respect to the platform. The third mode is 'drift then return'. OCARINA first records its original position. Next, it drifts for 30 minutes and cruises back to its original position, repeatedly. Fourth and last mode is called 'record position and route to follow'. The boat cruises for 30 minutes following the recorded route, and cruises back to its original position. Note that wave data cannot be inferred from recorded motion when OCARINA has its engine on.

OCARINA is controlled via a remote control with 400 m range, or via satellite (Iridium system). Currently, satellite communication is only used for getting the current position of OCARINA and to proceed to its recovery rather than for guidance, given its small operating range, which is ~10 km.

3. The FROMVAR 2011 experiment

The FROMVAR project was devoted to the study of the Ushant tidal front in Mer d'Iroîse, off the west coast of Brittany, France, which results from the tidal actions and air-sea interactions (http://wwz.ifremer.fr/epigram/Acces-aux-donnees/Campagnes/FROMVAR, and Le Boyer et al., 2009). FROMVAR aimed at understanding the hydrological structure, the currents and the dynamical processes associated with this front. The project consisted of several one-to-two-week experiments every year since 2007. OCARINA was part of the last experiment, from 10 to 15 September 2011. In addition to OCARINA, air-sea flux data were acquired during every experiment, on board the French Institut National de l'Univers (INSU) R/V 'Côtes de la Manche' (CDLM hereafter), which is 26 m long. Unfortunately, not enough data were sampled in order to get reliable comparison between the two platforms. Therefore, the CDLM flux estimates will not be discussed in the present paper.

During FROMVAR, OCARINA was deployed eight times in five days, from 30 minutes to more than two hours each time. The locations at which OCARINA was deployed during the cruise of the CDLM are represented on Figure 4. Bathymetry ranged from ~20 m to ~120 m. Several deployments were conducted in the Bay of Douarnenez, thus not in open sea conditions. The fourteen different weather conditions (referred to as fourteen cases in the following) encountered during the experiment were from low to moderate wind speeds, from ~1 ms^{-1} to ~8 ms^{-1}, as reported in Table 2 (column 6). The surface boundary layer was either unstable or stable, with sometimes strong thermal stratification (Table 2). In the most stable case, the maximum difference between air temperature and sea surface temperature was equal to +1.1°C, with the formation of gravity waves in the boundary layer, as independently inferred from LIDAR measurements. Significant wave heights (H hereafter) were estimated with OCARINA data. H was calculated as four times the standard deviation of the elevation (η, which is the difference between the actual vertical position and the mean sea level), an output from the MTI-G instrument. The H estimates ranged from 1.1 m to 3.3 m. OCARINA significant wave height estimates were already compared to two buoy data sets in the report by Morisset et al. (2013). Their conclusion is that OCARINA underestimates the wave height for wave lengths smaller than four meters, which was expected because it is on the order of

the size of OCARINA. It is likely that then physical configuration of OCARINA and its dynamical interaction with the surface acts as a lowpass filter with respect to the recorded motion of small spatial wavelengths. A further comparison of OCARINA derived wave heights to output fields from the PREVIMER pre-operational prediction system for coastal environment (Lecornu and De Roeck, 2009, see also http://www.previmer.org/en) is presented in Figure 5a. Although it is not a strict validation of OCARINA data, PREVIMER was chosen as it was the only available source for estimating wave characteristics in the investigated area. The root mean square (rms hereafter) deviation between PREVIMER and OCARINA estimates of H is 0.3 m, which is acceptable, although small wave heights do not compare well. Note that the outliers on Figure 5a correspond to small and short waves in shallow water, which could be misrepresented both in the model and in OCARINA data. In order to assess the accuracy of H estimates for small but long waves, an additional comparison based on data collected in 2010 in the vicinity of Porquerolles Island (near Marseille, France) and Cap Ferret (near the Landes coast, France) is presented on Figure 5b. The values of H deduced from OCARINA data are compared to reference buoy data (buoy Porquerolles, ID #61004 and buoy Cap Ferret, ID #62064). The rms deviation between OCARINA and buoy estimates is 0.06 m, which is encouraging.

4. Distortion and motion characteristics

a. Flow distortion

Simulations were performed following the method described in Bourras et al. (2009). The fluid simulation software used is an industry standard named “Fluent”, from the ANSYS Company. The air volume that encompasses the OCARINA surface is 20 m long by 20 m wide by 10 m tall. This air volume is gridded with an unstructured mesh, based on tetrahedral elements, the size of which is smaller close to OCARINA. Several flow solvers including laminar and Reynolds stress model were tested. They gave qualitatively similar results. The results presented in Figure 6 are based on laminar simulations. Even in the worst case scenario, when the wind comes across OCARINA, vertical wind distortion should be ~3° at 1.5 m above the platform, as shown on Figure 6, which is less than half what is found for a 50-80 m long R/V, i.e. 7-10° (Bourras et al., 2009). In addition, distortion is smaller than 3° if the wind comes from other directions, which is an advantage over large R/Vs for which 6° is a minimum value that increases with the wind angle (Bourras et al., 2009). At the location of the portside meteorological mast (at 1-m height), the simulations indicate that distortion is on the same order of magnitude as for the vertical mast at 1.5 m. Note that in the simulations, OCARINA is assumed to be horizontal, which is the case for averages over time periods larger than some minutes. For shorter time periods, steady simulations would not be meaningful without taking into account both waves and OCARINA motion, which was not attempted.

According to FROMVAR observations, the mean vertical wind angle is 1.27° at the height of 1.5 m, as can be calculated from the angle values reported in Table 3 for the fourteen cases. Thus, the actual distortion angles are ~2° smaller than in the simulations presented above, which is encouraging. Similarly, the mean vertical velocity is 0.12 ms^{-1}, which is small compared to the velocity commonly found for research vessels, i.e. ~1 ms^{-1} (e.g. Bourras et al., 2009). It was checked that rotation of the wind vector of an angle that would cancel the mean value of the vertical wind component had a very limited impact on the estimates of

turbulent fluxes. It was concluded that it was not necessary to apply any distortion correction to OCARINA data.

b. Motion and its impact on wind measurements

Understanding how OCARINA moves on waves as a function of data sampling frequency is important because its shape and characteristics are different from other platforms. A typical wind and motion power spectrum is presented on Figure 7, for a 20-min interval that started on 2011/09/14 at 7:22 UTC when the swell was largest. The relative wind curve (in black) reveals two broad peaks that correspond to swell (centered on 0.1 Hz) and to the resonating frequency of OCARINA (at 1 Hz), respectively. The swell peak corresponds well to the peak in the power spectrum of η (green curve). In order to assess whether the relationship between swell and wind is physical or is due to variations of ship attitude and motion, we performed a true wind calculation, as fully described in Pédreros et al. (2002). After application of the correction, the power spectrum of the along wind component (blue curve on Figure 7) still presents a large peak at the frequency of the swell. As a result, the peak in wind is actually related to a physical relationship between wind and swell. This relation will be further analyzed in section 6.

The peak at 1 Hz on Figure 7 fits the linear velocity of OCARINA (deduced from roll angular velocity). After application of the correction, the peak is almost totally removed, which confirms that it was almost totally related to OCARINA motion.

Note the presence of a sharp peak at 10 Hz on Figure 7 that presumably corresponds to a flexion mode of the turbulent mast, which is a vertical carbon tube, in interaction with the structure of the platform.

The frequency range that can be used for estimating fluxes with the spectral method, or ID method in the following (Dupuis et al., 1997) is restricted to 3-9 Hz without correction, because in this range, the slope of the linear fit to data is the closest to a value of -5/3, which is nominal for applying the ID method. Note that after correction, the frequency range could be extended to frequencies in the 1-3 Hz range. However, only the 3-9 Hz band was used because it is sufficient for applying the ID method.

In contrast, for the EC method the maximum frequency of the wind or temperature data was restricted to 2 Hz with a first order low pass filter. This cut-off frequency corresponds to the end of the turbulence production range and to the beginning of the ‘clean’ inertial range, as illustrated on Figure 7. The filter was applied so as to avoid parasite signals such as the peak at 10 Hz on Figure 7. The impact of this filter was tested: if no filter was applied, then the EC method slightly overestimated the other fluxes. In addition, the application of the filter improved the comparisons to the bulk and ID methods.

5. Air-sea fluxes

Friction velocity (u^*) is related to the turbulent momentum flux, which is $\begin{pmatrix} \overline{u'w'} \\ \overline{v'w'} \end{pmatrix}$ in vector form, where u', v', and w' are the turbulent fluctuations of the wind in the along wind, in the cross wind, and in the vertical directions, respectively. The relation between u^* and the momentum flux is written as,

$$u^* = \left(\overline{u'w'}^2 + \overline{v'w'}^2 \right)^{\frac{1}{4}}$$

In the present paper, u^* was estimated with the bulk method, the ID method, and the EC method. The comparisons between the three estimates of u^* are encouraging in spite of the small number of points available, as shown in Figure 8. The rms deviation is 0.02 ms^{-1} both between EC u^* and bulk u^*, and between EC u* and ID u^*, which is good compared to R/V data (e.g. Pedreros et al., 2003). However, the slope of the linear fit between EC u^* values and bulk or ID u^* estimates, is 1.1-1.07, which implies that large EC u^* values are higher compared to the bulk and ID values of u^*.

In order to analyse why there is an overestimation for EC u* values, the cospectra of $-u'w'$ were calculated as a function of a normalized frequency (fz/U) and the experimental values found were compared to the empirical universal model of Kaimal et al. (1972) as shown in Figure 9. Cases with a similar behaviour were grouped together, namely moderate wind (Figure 9a,b and Table 2, rows 1-6 and 11-13), light wind and unstable conditions (Figure 9c and Table 2, line 10), light wind and stable conditions (Figure 9d and Table 2, rows 7-9), and no wind and stable conditions (Figure 9e and Table 2, row 14). On Figure 9a,b, there is an overall good agreement between the model of Kaimal et al. (1972) and OCARINA data. However, at time periods larger than 20 sec, the data have higher spectrum power than the model. In contrast, in light wind conditions (Figure 9c,d), model and data do not agree well. Specifically in stable cases, (Figure 9d,e) there is a peak in the OCARINA cospectra at fz/U =0.5-0.9, which is not present in the model. As a test, the EC time series of u' and w' were high passed with decreasing cut-off time periods (T) from 1 000 sec to 20 sec. For each test, the rms and systematic deviations between EC and bulk u* estimates were checked. The best agreement was found with T=35 sec, which is shown on Figure 10b,c. The rms deviation between the different u^* estimates is 0.01 ms^{-1}, and the slope of linear fit is 0.96-0.99, which is rather good. This indicates for this platform, a strong sensitivity on the cut-off period retained for estimating the covariance fluxes.

No humidity fluctuations were available with the set of instruments installed on OCARINA during FROMVAR. As a result, the latent heat flux could not be estimated with the EC method or the ID method. As the sensible heat flux also depends on humidity, a virtual sensible heat flux, better known as the buoyancy flux, was calculated instead. It is referred to as *Hsv* hereafter.

The comparisons between *Hsv* estimated with the EC method, with the ID method and with the bulk method are shown on Figure 10d-f. Although there are not enough points of comparison to draw firm conclusions, the comparisons between EC and bulk *Hsv* values are encouraging (Figure 10d,e). The rms deviation between EC (ID) and bulk *Hsv* values is 2.5 (3.3) Wm^{-2}, which is reasonable. However, the results presented on Figure 10e indicate that in

stable cases the large negative ID *Hsv* values are overestimated in comparison to the bulk values. The comparison between EC and ID *Hsv* values further reveals that the range of ID *Hsv* values is globally too large with respect to the range of EC *Hsv* values, as shown on Figure 10f. The sensitivity of the bulk estimates to several input parameters inside the COARE algorithm (Fairall et al., 2003), namely jwave, jwarm and jcool, which relate to the parameterization of the aerodynamic roughness length and to the skin minus bulk sea temperature calculation, respectively, was further tested. This had little impact on the results. We also attempted to account for the surface current from PREVIMER analyses in the calculation of the bulk estimates but this also had little impact on the results. Thus, for this platform, we recommend for *Hsv* to use EC or bulk estimates, but not the ID estimates of *Hsv.*

As two anemometers were available on OCARINA (at 1 and 1.5 m), we also attempted to estimate u* values with the profile method, which is written as,

$$u^* = \frac{\kappa}{\left(\ln(1.5) - \Psi\left(\frac{1.5}{L}\right) + \Psi\left(\frac{1}{L}\right)\right)}\left(U_{1.5} - U_1\right)$$

where κ is the Von Karman constant, equal to 0.4, L is the Monin-Obukhov length, and the Ψ function chosen follows Smith (1988). Comparisons between estimates of u^* calculated according to the profile method and to the bulk method are presented in Figure 11. As shown in Figure 11, profile and bulk methods produce comparable u^* estimates when the wind blows from the port side of OCARINA. We hypothesize that if the wind is coming from the starboard side, the starboard mast may disturb the wind at the location of the WXT-520 weather station (which is then in the wake of the starboard mast). The good performance of the profile method is uncommon, because it is challenging to apply it at sea for two reasons: either data are sampled at heights that are too large, in which case the wind variations between the two levels is too small to be detected (because the curvature of the log profile is large only at small heights), or because of height dependent flow distortion which is difficult or impossible to correct. Note that the results were hardly changed if stability was accounted for or not in the calculation, as also shown on Figure 11, which possibly results from the small w, thus a small z/L. This suggests that in certain conditions the wind profiles estimated on OCARINA are very reasonable.

Along and cross wind components of the EC stress define the so-called stress angle $\theta = \tan^{-1}\left(\frac{\overline{v'w'}}{\overline{u'w'}}\right)$. The angle θ was plotted versus the horizontal wind speed on Figure 12. As shown on Figure 12, the scatter is large if wind speed is smaller than 6 ms^{-1}. In contrast, if wind speed is larger than 6 ms^{-1} then wind and stress are almost aligned with each other, which fits well with existing data (e.g. Grachev et al., 2001), in spite of the very limited number of points available for comparison.

6. Wind-wave interaction

In this section, we investigate the relation between the instantaneous horizontal wind modulus (U) calculated with respect to the ground (as opposed to the wind relative to OCARINA) and η.

Eight cases are available for analysis, namely four cases with wind and swell travelling in the same direction, i.e. cases 7 to 10 in Table 2, and four cases when swells are travelling in opposite direction to the winds, i.e. cases 11 to 14 in Table 2. Each case corresponds to a time interval of twenty minutes, which corresponds to 60 000 samples.

First, we estimated the dominant wave period (T_0) of the swell, as the inverse of the frequency (f_0) that corresponded to the maximum of the power spectrum of η, over twenty minute intervals. Next, the f_0 estimates were used to calculate the dominant wave length (L_∞), the wave number (k), and the phase speed of waves at the peak frequency (c) using the linear wave dispersion relationship, with the hypotheses that wave amplitude (a) is small and that water column is deep. Wave age $\left(\frac{c}{U}\right)$ and wave steepness ($a.k$) were next calculated, the value of a being approximated as $\frac{1}{2}\mathrm{H}$. The maximum of the orbital speed $(V_{orb})_{\max}$, which is the value of the orbital speed at the crests of the waves, was finally estimated as,

$$(V_{orb})_{\max} = \pi \frac{\mathrm{H}}{T_0} \exp\left(\frac{2\pi}{L_\infty} a\right),$$

There could be significant differences between the calculated value of $(V_{orb})_{\max}$ and its actual value, but unfortunately it was not possible to get a more direct estimate of it because no log instrument (which would measure the speed of the platform with respect to the sea surface) was available on OCARINA during FROMVAR. The above mentioned wave characteristics are summarized on Figure 13.

The existence of a relationship between wind and waves was investigated by studying the spectral coherence (coh) and the phase (φ) between η and U. The values of coh and φ were computed as,

$$coh = \frac{\left\langle DFT(U).conj(DFT(\eta))\right\rangle^2}{\left\|DFT(U)\right\|^2.\left\|DFT(\eta)\right\|^2}$$

$$\varphi = Arg\left(\frac{DFT(\eta)}{DFT(U)}\right)$$

where DFT is the Discrete Fourier Transform, and the < > operator denotes ensemble averaging. Eight spectra of coh and φ are shown on Figure 14, for example. In order to summarize the results for the eight cases, and to test the detection of the coherence between coh and φ, the mean value of coh was calculated in the spectral range of the swell (i.e. between 0.06 Hz and 0.18 Hz for cases 7-10, and between 0.08 Hz and 0.15 Hz for cases 11-14), and then it was divided by the standard deviation (σ_f) of coh. As shown on Figure 15a, coh is larger than 2σ for each case, which means that it is meaningful to interpret the phase between η and U in the frequency range of the swell, as shown on Figure 15b.

Cases 7 to 10 present a phase shift of 3.0° between wind and waves. For cases 11 to 14, the average phase shift is even smaller, i.e. 1.9°, as can be checked on Figure 15b. The phase shift

φ between η and the wind relative to the waves, which is defined as $\overrightarrow{U_r} = \vec{U} - \vec{c}$, is best illustrated on Figure 16, averaged over all cases. As shown on Figure 16, the wind maximum occurs near the crest of the swell, but with a small phase shift on the side of the windward face. There could result from errors associated with the values of φ given above. We expect that the correction of the motion of OCARINA (based on accelerometer and gyroscope data) is the most important source of error. In order to check the impact of this source of error on φ, we performed new calculations of φ with a perturbation factor in the motion correction, in a ratio of -30% to +30%, which is a worst case scenario. The result was a shift of phase of ± 8° to ± 13°. Surface current was taken into account in the calculation of *U*. We also checked the impact of an error on the value of the current. If the current is not taken into account, then the values of φ are modified by -1° only, thus current has little impact on the phase found. Finally, we found that the average value of φ was $+2.4° \pm 14°$.

Since real waves are not pure monochromatic sinusoidal functions, it is difficult to illustrate the mean wind profile along the phase of the wave. Instead, we analyzed the statistical relation between *U* and η. The time series of *U* and η were band filtered in the spectral region of maximum coherence, i.e. between 0.06 Hz and 0.18 Hz for cases 7-10, and between 0.08 Hz and 0.15 Hz for cases 11-14. Next, the time series of *U* and η were normalized as $U_n(t) = \frac{U(t)}{4\sigma_U}$ and $\eta_n(t) = \frac{\eta(t)}{4\sigma_\eta}$, and then were shifted according to φ. Next the correlation coefficient and the slope α of the first degree linear fit between U_n and η_n were calculated. As shown on Figure 17, there is a statistical linear relationship between U_n and η_n, even though α varies by more than 50% depending on the case under consideration. Wind amplitude was estimated as $2\sigma_U$. Its values are plotted on Figure 17c. On average, we found that $2\sigma_U$=0.9 ms^{-1} for following-swell cases, and $2\sigma_U$=1.4 ms^{-1} for counter-swell cases, which is comparable to the maximum orbital speed values represented on Figure 13. This supports the idea that OCARINA is well adapted to further study the wave induced wind undulation and stress.

7. Discussion

A new design of platform is proposed for determining air-sea turbulent fluxes, surface heat budget, and some aspects of wave characteristics. OCARINA design and the results found in the present paper with OCARINA data are discussed hereafter; despite only a limited test set of fourteen cases was available for validating the use of the platform and for investigating wave characteristics, turbulent fluxes and wind-wave interactions.

a. Design

It was observed that the platform motion characteristics were fully compatible with the determination of fluxes (section 4b). OCARINA orients itself perpendicular to the relative wind, which is not the best configuration for air flow distortion. However, distortion is still small, ~3°, as was shown in section 4a.

The proposed design is obviously not the only possible response to the design criteria mentioned in section one. Furthermore, the design is probably not better in terms of

aerodynamic performance than what can be obtained by the ASIS buoy (Graber et al., 2000), at least for measurements performed at heights larger than 1.5 m.

With the chosen configuration, the three main following criticisms can be made. First, a host ship is still required to deploy and recover the platform. Second, it would be impossible to get time series longer than a day with no gaps because batteries would have to be charged after twelve hours. Last, a light design means a very limited payload and electric power, thus the range of instruments that can be installed on OCARINA is limited. Electric power would be even more limited in cold regions, where batteries would be less efficient. On the contrary, OCARINA was recently tested with success in tropical regions, with no overheating issues.

Wave heights for wave lengths larger than the size of the platform could be inferred from the motion of the platform with a reasonable accuracy, on the order of 0.1 m in rms. However, as opposed to systems like ASIS, OCARINA cannot currently sample short waves. In addition, directional spectra of waves (hodographs) are presently not available. Note that ancillary gauges could be installed for obtaining these data, in the future.

Another limitation of OCARINA is that it drifts rather quickly under the effects of wind and surface current (<0.5 ms^{-1} drift in a 10 kts wind). Drift is an issue that must be taken into account while planning the mission of the host ship, or if obstacles are present like in coastal areas. Adding a drogue (parachute) to limit the drift of OCARINA was not attempted as it could affect the motion of OCARINA, thus the quality of the wave height estimates.

While designing OCARINA, a major concern was the water intrusion on the instruments so close to the waves. Water could affect the quality of sonic anemometer and radiation data. In practice, this did not happen for winds up to 17 kts (recorded in the bay of Douarnenez at the beginning of the FROMVAR experiment) and for waves up to 3.3 meters (on 14 September 2011, during FROMVAR), possibly due to its light weight, its stability, its small size, and the subsequent constant height of the instruments above water. However, this could be problematic for steep waves and large spray generation. No simulation was made to further assess the maximum acceptable wave steepness or height that OCARINA could withstand.

b. Air-sea fluxes

Four flux estimation methods were applied, namely the EC method, the ID method, the bulk method, and the profile method (for u^* only). Only the friction velocity and the buoyancy flux were discussed in the present paper, as no instrument was available for measuring humidity fluctuations during the experiment. Cospectra of $u'w'$ exhibited similar behaviour as the empirical model of Kaimal et al. (1972) for cases of unstable surface boundary layer. However, in the lower frequency range, OCARINA cospectra were higher than those of' the model. In addition, it was noticed that the comparisons between EC u^* estimates and bulk and ID u^* estimates were improved by a factor up to two if the lower parts of the spectra were filtered out in the EC method, with a cut-off time period of 35 sec. Under stable conditions or in low wind conditions, the OCARINA cospectra of $u'w'$ were significantly different from the Kaimal et al. (1972) model, although the corresponding u^* estimates were in good agreement with the other methods.

As OCARINA is a wave follower, the EC u^* values measured at constant height above the surface could slightly differ from the EC u^* values that would have been be measured at constant altitude (see the relationship in Grare et al., 2013, Appendix A). The order of magnitude of the differences will be checked in a future work.

We found that the bulk buoyancy flux compared well to EC estimates of the flux. In contrast, the buoyancy flux estimates from the ID method did not have a good fit to EC fluxes or bulk fluxes, especially in stable conditions. Unfortunately, too few points of comparison were available to draw firm conclusions. In a future work, this issue will be further investigated. The exponents of the inertial ranges of wind and temperature spectra, the critical Richardson number and z-less parameterization will be tested, and compared to recent results of Grachev et al. (2012).

c. Wind and waves

It was shown that the alignment between stress and the mean wind direction was good when wind speed was larger than 6 ms^{-1}, which is consistent with earlier results (Grachev et al., 2001). Wind and swell were spectrally coherent for eight cases. Furthermore, statistical linear relationships were found between wind variations and surface elevation. The phase shift between wind and swell was $+2.4° \pm 14°$ (average of following and counter swell cases). Currently, there is a lack of data showing the phase between wind and surface elevation in the open sea. However, numerical models have been run (e.g. Sullivan et al., 2008), and wind tunnel data (Grare et al., 2013) as well as theoretical models (Kudryavtsev et al., 2001, Semedo et al., 2009) were already published on the subject. According to the simulations made by Sullivan et al. (2008, Page 1231, Figure 5), wind should be in phase with the elevation, i.e. wind accelerates on wave crests and slows down in wave troughs, consistent with what was found for OCARINA. Following previous authors (Belcher and Hunt, 1993; Cohen and Belcher, 1999), a model of airflow above waves was proposed by Kudryavtsev et al. (2001), in which the atmospheric layer was split into two regions, the inner and the outer region. The altitude l of the limit separating both regions was defined by the following expression,

$$kl = \frac{2\kappa u^*}{|U(l)|}$$

According to OCARINA data, the value of l is ~0.9 m, which means that OCARINA data at 1.5 m are made at the bottom of the outer region. According to the simulations and to the validation data of Kudryavtsev et al. (2001), as well as of Sullivan et al. (2008), wind would be smaller in the trough of the waves than over the crests, which is in qualitative agreement with the present data. However, one would expect a larger phase shift value, i.e. wind would be at maximum on the windward sides of the waves –in advance with respect to the crest-. The phase would also increase with wave steepness, and decrease with wave age (Grare et al. 2013). In the present paper, wave age is large, i.e. 2-12, and wave steepness is rather small, from 0.03 to 0.06, which might explain the small value of the phases found. No clear relationship was found between wind amplitude and orbital velocity, although they are of compatible magnitude.

An effort to add a humidity fluctuation measurement instrument, a log, and a set of wave gauges to OCARINA is in progress. In its present configuration, OCARINA was recently deployed during the SPURS STRASSE experiment (e.g. Reverdin et al. 2013), providing 120 hours for data collection. Data processing and analysis is ongoing at LATMOS (R. Cambra), and will be the object of a future paper. The masts of OCARINA will be adapted to a WaveGlider in the near future (http://liquidr.com).

Acknowledgements
The authors are grateful to the captains and the crew of the INSU R/V "Côtes de la Manche", DT-INSU at la Seyne sur mer, B. Zucchini at IRPHE, and F. Rémy at Ecole Centrale de Marseille for their help. The development of OCARINA was funded by several sources that included IPSL, UPMC-EMERGENCE, and LATMOS.

References

Anctil, F., M. A. Donelan, W. M. Drennan, and H. C. Graber, 1964: Eddy-Correlation Measurements of Air-Sea Fluxes from a Discus Buoy, *J. Atmos. Oceanic Technol.*, **11**, 1144-1150.

Berry, D. I., E. C. Kent, and P. K. Taylor, 2004: An analytical model of heating errors in marine air temperatures from ships. *J. Atmos. Oceanic Technol.*, **21**, 1198-1215.

Bourras, D., et al., 2009: Turbulent air-sea fluxes in the Gulf of Guinea during the AMMA experiment. *J. Geophys. Res.*, **114**, C04014.

Brut A., A. Butet, P. Durand, G. Caniaux, and S. Planton, 2005: Air-sea exchanges in the Equatorial area from the EQUALANT99 dataset: bulk parameterizations of turbulent fluxes corrected for airflow distortion. *Q. J. R. Meteorol. Soc.*, **610**, 2497-2538.

Christensen, K. H., J. Rohrs, B. Ward, I. Fer, G. Brostrom, O. Saetra, O. Breivik, 2013: Surface wave measurements using a ship-mounted ultrasonic altimeter. *Methods in Oceanography*, Early online release, doi:10.1016/j.mio.2013.07.002, 15pp

Donelan, M. A., F. W. Dobson, S. D. Smith, and R. J. Anderson, 1993: On the Dependence of Sea Surface Roughness on Wave Development. *J. Phys. Oceanogr.*, **23**, 2143-2149.

Donelan, M. A., W. M. Drennan, and K. B. Katsaros, 1997: The Air–Sea Momentum Flux in Conditions of Wind Sea and Swell. *J. Phys. Oceanogr.*, **27**, 2087-2099.

Donelan, M. A., A. V. Babanin, I. R. Young, M. L. Banner, and C. McCormick, 2005: Wave-Follower Field Measurements of the Wind-Input Spectral Function. Part I: Measurements and Calibrations. *J. Atmos. Oceanic Technol.*, **22**, 799-813.

Drennan, W. M., H. C. Graber, and M. A. Donelan, 1999: Evidence for the Effects of Swell and Unsteady Winds on Marine Wind Stress. *J. Phys. Oceanogr.*, **29**, 1853-1864.

Dupuis, H., P. K. Taylor, A. Weill, and K. Katsaros, 1997: Inertial dissipation method applied to derive turbulent fluxes over the ocean during the Surface of the Ocean, Fluxes and Interactions with the Atmosphere/Atlantic Stratocumulus Transition Experiment (SOFIA/ ASTEX) and Structure des Echanges Mer-Atmosphere, Proprietes des Heterogeneites Oceaniques: Recherche Experimentale (SEMAPHORE) experiments with low to moderate wind speeds. *J. Geophys. Res.*, **102**, 21,115–21,129.

Edson, J. B., C. W. Fairall, P. G. Mestayer, and S. E. Larsen, 1991: A study of the inertial-dissipation method for computing air-sea fluxes. *J. Geophys. Res.*, **96**, 0148-0227.

Edson, J. B., A. A. Hinton, K. E. Prada, J. E. Hare, and C. W. Fairall, 1998: Direct Covariance Flux Estimates from Mobile Platforms at Sea, *J. Atmos. Oceanic Technol.*, **15**, 547-562.

Edson, J. B., T. Crawford, J. Crescenti, T. Farrar, N. Frew, G. Gerbi, A. Plueddemann, J. Trowbridge, R. Weller, A. J. Williams, C. Helmis, T. Hristov, L. Shen, D. Khelif, A. Jessup, H. Jonsson, M. Li, L. Mahrt, E. Skyllingstad, D. Vickers, W. McGillis, C. Zappa, T. Stanton, Q. Wang, P. Sullivan, J. Sun, S. Wang, J. Wilkin, and D. K. P. Yue, 2007: The Coupled Boundary Layers and Air–Sea Transfer Experiment in Low Winds, *Bull. Amer. Meteor. Soc.*, **88**, 341-356.

Fairall. C. W., E. F. Bradley, J. E. Hare, A. A. Grachev, and J. B. Edson, 2003: Bulk parameterisations of air-sea fluxes: updates and verification for the COARE algorithm. *J. Climate*, **16**, 571-591.

Graber H. C., E. A. Terray, M. A. Donelan, W. M. Drennan, J. C. Van Leer, and D. B. Peters, 2000: ASIS—A New Air–Sea Interaction Spar Buoy: Design and Performance at Sea. *J. Atmos. Oceanic Technol.*, **17**, 708-720.

Grachev, A. A, C. W. Fairall, J. E. Hare, and J. B. Edson, 2001: Wind Stress over Sea Waves, *11th Conference on Interaction of the Sea and Atmosphere*.

Grachev, A., A., E. L. Andreas, C. W. Fairall, P. S. Guest, and P. O. G. Persson, 2012: The Critical Richardson Number and Limit of Applicability of Monin-Obukhov Similarity Theory in the Stable Atmospheric Boundary Layer, *20th Symposium on Boundary Layers and Turbulence.*

Grare L., W. Peirson, H. Branger, W. Walker, J. P. Giovanangeli, and V. Makin, 2013: Growth and dissipation of wind forced deep water waves. *J. Fluid Mech.*, **722**, 5-50.

Kaimal, J. C., J. C. Wyngaard, Y. Izumi, and O. R. Coté, 1972: Spectral Characteristics of surface-layer turbulence, *Q. J. R. Meteorol. Soc.*, **98**, 563-589.

Katsaros, K. B., 1980: The aqueous thermal boundary layer. *Bound.-Layer Meteor.*, **18**, 107–127.

Katsaros, K. B., M. A. Donelan, and W. M. Drennan, 1993: Flux measurements from a SWATH ship in SWADE. *J. Mar. Syst.*, **4**, 117-132.

Kolmogorov, A. N., 1941: The local structure of turbulence in incompressible viscous fluid for very large Reynolds numbers. *Proc. USSR Academy of Sciences*, **30**, 299–303.

Kudryavtsev, V. N., V. K. Makin, and J. F. Meirink, 2001: Simplified Model Of The Air Flow Above Waves. *Bound.-Layer Meteor.*, **100**, 63-90.

C. Le Boyer, G. Cambon, N. Daniault, S. Herbette, B. Le Cann, L. Marié, P. Morin, 2009: Observations of the Ushant tidal front in September 2007, **29**, 1026-1037.

Lecornu, F., and Y.-H. De Roeck, 2009: PREVIMER - Coastal observations and forecasts. *Houille blanche, revue internationale de l'eau,* **3**, 60-63.

Liu, W. T., K. B. Katsaros, and J. A. Businger, 1979: Bulk Parameterization of Air-Sea Exchanges of Heat and Water Vapor Including the Molecular Constraints at the Interface. *J. Atmos. Sci.*, **36**, 1722–1735.

Monin, A. S., A. M. Obukhov, 1954: Basic laws of turbulent mixing in the surface layer of the atmosphere. *Tr. Akad. Nauk SSSR Geofiz.*, **24**, 163–187.

Miller, S. D., T. S. Hristov, J. B. Edson, C. A. Friehe, 2008: Platform Motion Effects on Measurements of Turbulence and Air–Sea Exchange over the Open Ocean. *J. Atmos. Oceanic Technol.*, **25**, 1683-1694.

Morisset, S., and G. Reverdin, Prototype drifter study: “Tag proto” (SMRULOCEAN), internal report, LOCEAN-UMPC, 2011, 38 pp., in French. Available upon request from simon.morisset@locean-upmc.ipsl.fr.

Pedreros, R., G. Dardier, H. Dupuis, H. C. Graber, W. M. Drennan, A. Weill, C. Guérin, and P. Nacass, 2003: Momentum and heat fluxes via the eddy correlation method on the R/V L'Atalante and an ASIS buoy. *J. Geophys. Res.*, **108**, 3339.

Popinet, S., M. Smith, and C. Stevens, 2004: Experimental and Numerical Study of the Turbulence Characteristics of Airflow around a Research Vessel. *J. Atmos. Oceanic Technol.*, **21**, 1575-1589.

Reverdin, G., S. Morisset, D. Bourras, N. Martin, A. Lourenço, J. Boutin, C. Caudoux, J. Font, and J. Salvador, 2013: Surpact: A SMOS surface drifter for air-sea interaction. *Oceanography*, 26, 48-56.

Sahlée, E., W. M. Drennan, H. Potter, and M. A. Rebozo, 2012: Waves and air-sea fluxes from a drifting ASIS buoy during the Southern Ocean Gas Exchange experiment. *J. Geophys. Res.*, **117**, C08003.

Semedo, A., Ø. Saetra, A. Rutgersson, K. K. Kahma, H. Pettersson, 2009: Wave-Induced Wind in the Marine Boundary Layer. *J. Atmos. Sci.*, **66**, 2256–2271.

Smedman, A., U. Högström, E. Sahleé, W. M. Drennan, K. K. Kahma, H. Pettersson, and F. Zhang, 2009: Observational Study of Marine Atmospheric Boundary Layer Characteristics during Swell. *J. Atmos. Sci.*, **66**, 2747-2763.

Smith, S. D., 1988: Coefficients for sea surface wind stress, heat flux, and wind profiles as a function of wind speed and temperature. *J. Geophys. Res.*, **93**, 15467–15472.

Soloviev, Y. P., and V. N. Kudryavtsev, 2010: Wind-Speed Undulations Over Swell: Field Experiment and Interpretation. *Bound.-Layer Meteor.*, **136**, 341-363.

Sullivan, P. P., J. B. Edson, T. Hristov, J. C. McWilliams, 2008: Large-Eddy Simulations and Observations of Atmospheric Marine Boundary Layers above Nonequilibrium Surface Waves. *J. Atmos. Sci.*, **65**, 1225–1245.

Weill, A., L. Eymard, G. Caniaux, D. Hauser, S. Planton, H. Dupuis, A. Brut, C. Guerin, P. Nacass, A. Butet, S. Cloché, R. Pedreros, P. Durand, D. Bourras, H. Giordani, G. Lachaud, and G. Bouhours, 2003: Toward a Better Determination of Turbulent Air–Sea Fluxes from Several Experiments. *J. Climate*, **16**, 600-618.

Weller, R. A., S. P. Bigorre, J. L. Jonathan, D. Ware, and J. B. Edson, 2012: A Surface Mooring for Air–Sea Interaction Research in the Gulf Stream. Part I: Mooring Design and Instrumentation. *J. Atmos. Oceanic Technol.*, **29**, 1363-1376.

Yelland, M. J., B. I. Moat, R. W. Pascal, and D. I. Berry, 2002: CFD Model Estimates of the Airflow Distortion over Research Ships and the Impact on Momentum Flux Measurements. *J. Atmos. Oceanic Technol.*, **19**, 1477-1499.

List of Tables

List of Figures

- Figure 13. Wave characteristics in open ocean conditions, during the FROMVAR experiment. On the x axis, one graduation corresponds to one 20-min bin.
- Figure 14. Spectra of coherence (left panels) and phase (right panels) between wind and sea surface elevation (eta). The greyed areas highlight the spectral regions of the swell, where the coherence is the largest. Phases are expressed in degrees. Each spectrum is calculated on a 20-min interval that starts at the time indicated in the panel title.
- Figure 15. Detection of coherence between U and η, for the spectral region of the swell (in panel a), and phase between U and η (panel b). In panel a, the coherence between U and η is detected because the values are larger than two for all cases.
- Figure 16. Phase shift φ between wave and phase averaged wind speed over cases 7-14.
- Figure 17. Statistical elements of the relation between normalized U_n and η_n (panels a,b) and wind amplitude (panel c).

Manufacturer	Instrument	data	unit	Sample rate	location
Vaisala	WXT520	Wind speed Air temperature Air pressure Relative humidity Precipitation	$m\ s^{-1}$ K hPa % mm	1 Hz	Port Mast
Kipp & Zonnen	CNR4	Downward solar flux Downward infrared flux Upward solar flux Upward infrared flux	$W\ m^{-2}$ $W\ m^{-2}$ $W\ m^{-2}$ $W\ m^{-2}$	1 Hz	Starboard Mast
Gill co.	R3-50	3D wind vector (u,v,w) Virtual temperature	$m\ s^{-1}$ K	50 Hz	Central Mast
Xsens	MTI-G	Longitude Latitude Altitude 3D angular rates 3D angles 3D linear speeds 3D accelerations 3D compass	Degree Degree m $rad\ s^{-1}$ rad $m\ s^{-1}$ $m\ s^{-2}$ arbitrary unit	50 Hz	Central float
Seabird	SBE-37	Sea surface temperature	K	1 Hz	Side of the central float

Table 1. Summary of the instruments installed on OCARINA, and list of the instrument locations and sampled data. Only the main recorded variables are reported above. Various ancillary data are also recorded for control and verification, such as temperature control or accuracy of GPS position data.

Case number	Date	Time	H (m)	SST – TA (K)	SSS (psu)	|Ur| (m s^{-1})	Wind-wave Conditions	Wind-wave angle (degrees)
1	2011/09/12	08:18:11	1.3	-1	35.383	8.7		-10
2		08:36:31	1.2	-1	35.375	8.3		-11
3		08:54:51	1.2	-1	35.357	8		-19
4		09:13:11	1.3	-0.8	35.344	7		-21
5		09:31:31	1.1	-0.7	35.380	7.2		-23
6		09:49:51	1.1	-0.7	35.393	6.7		-26
7	*2011/09/14*	*07:22:51*	*3.3*	*-0.5*	*35.538*	*2.6*	*Following swell*	*17*
8		*07:41:11*	*3.0*	*-0.4*	*35.537*	*2.7*		*17*
9		*07:59:31*	*3.2*	*-0.5*	*35.537*	*2.3*		*30*
10		*17:09:31*	*2.6*	*0.8*	*35.329*	*2*		*-50*
11	**2011/09/15**	**08:13:57**	**1.9**	**1.2**	**35.320**	**6.4**	**Counter swell**	**-173**
12		**08:32:17**	**2.1**	**1.2**	**35.277**	**6.4**		**-173**
13		**09:27:17**	**1.9**	**1.2**	**35.174**	**6.1**		**-183**
14		**13:25:37**	**1.6**	**-1.1**	**35.534**	**1.4**		**-240**

Table 2. Stability, wind and wave conditions during the FROMVAR 2011 experiment. Ur is the relative wind speed with respect to OCARINA. H is the significant wave height. SSS is the sea surface salinity in psu. SST is the sea surface temperature. TA is air temperature measured at 1m. The wind-wave angle is the difference between the angle of the true wind (wind with respect to ground) vector and the direction where the waves go. Both angles are counted counter clockwise.

Case	1	2	3	4	5	6	7	8	9	10	11	12	13	14
Angle (°)	1.1	1.6	1.6	1.4	1.6	1.5	0.9	1.2	0.5	0.2	0.5	0.4	1.3	3.1
w (ms^{-1})	0.26	0.24	0.23	0.17	0.20	0.17	0.04	0.05	0.02	0.01	0.06	0.04	0.14	0.06

Table 3. Mean vertical distortion angle and vertical wind component for each 20-min bin.

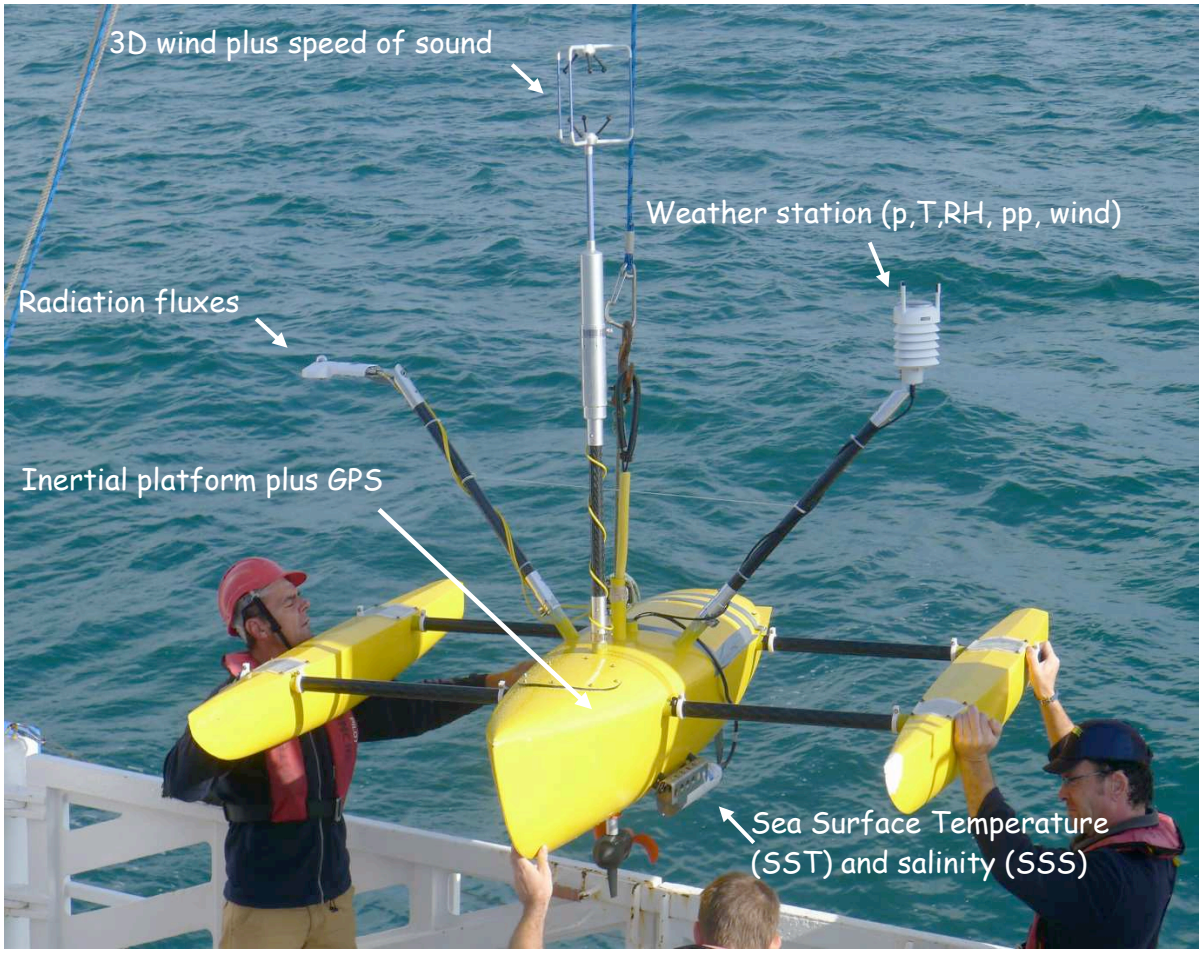

Figure 1. Deployment of OCARINA from the rear deck of the INSU R/V "Côtes de la Manche" during the FROMVAR 2011 experiment (Picture by H. Barrois, DT-INSU).

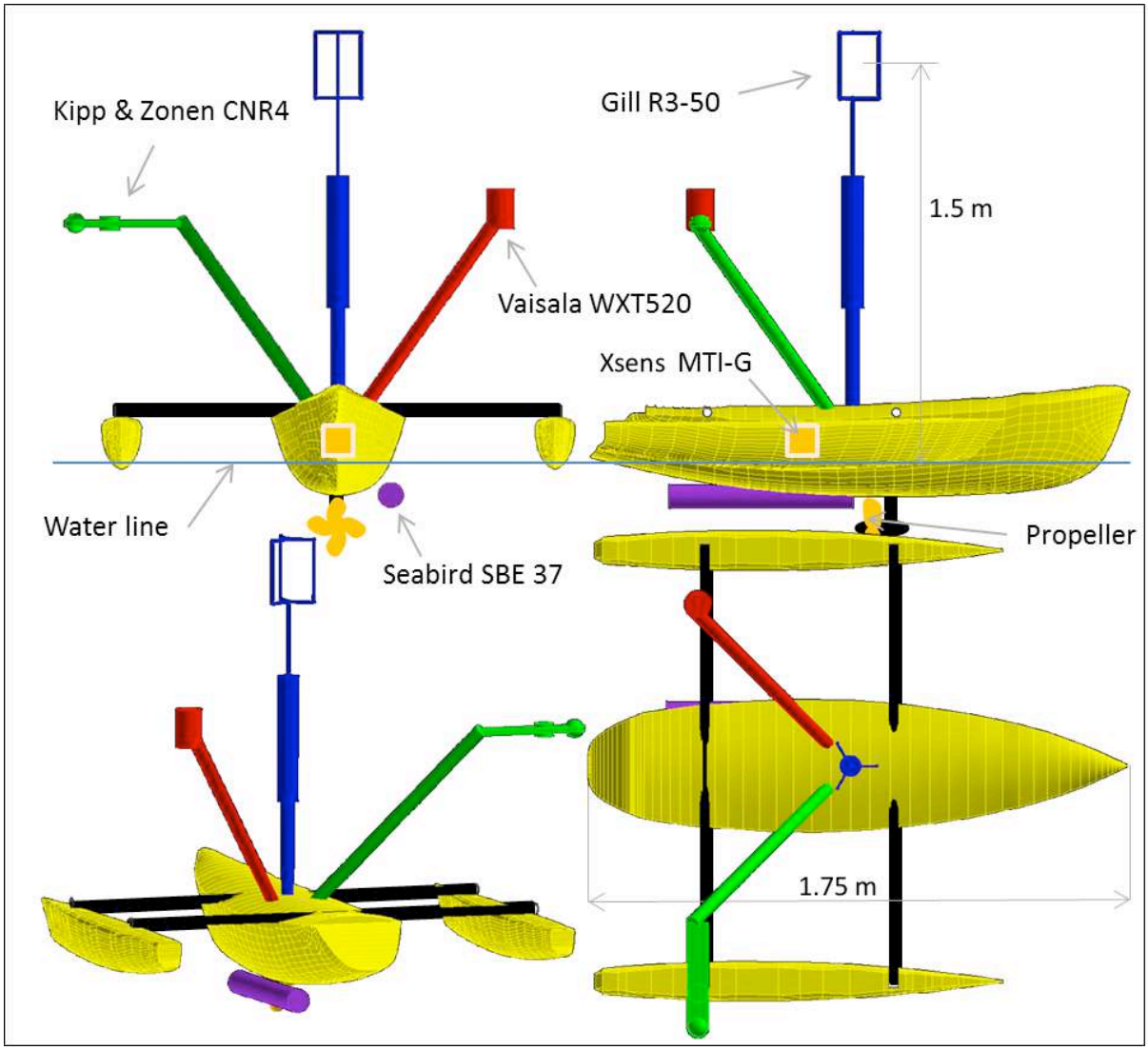

Figure 2. Conceptual view of the OCARINA platform.

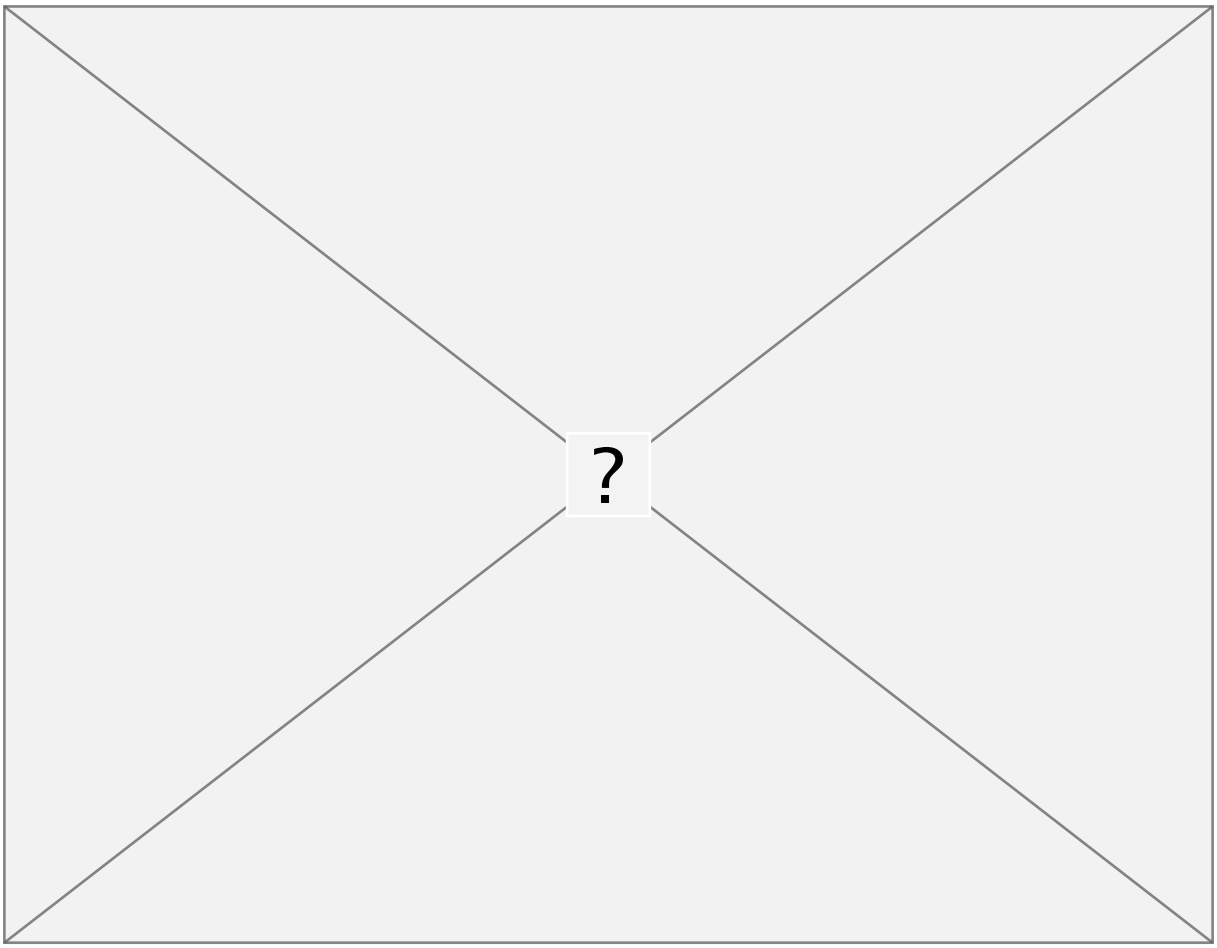

Figure 3. Flowchart of the data acquisition system. The data frames of each instrument (on top) are decoded. Next, a time tag based on a GPS clock is added, before the frames are stored in a buffer. When the buffer is full, its content is transferred to two SD cards, in parallel.

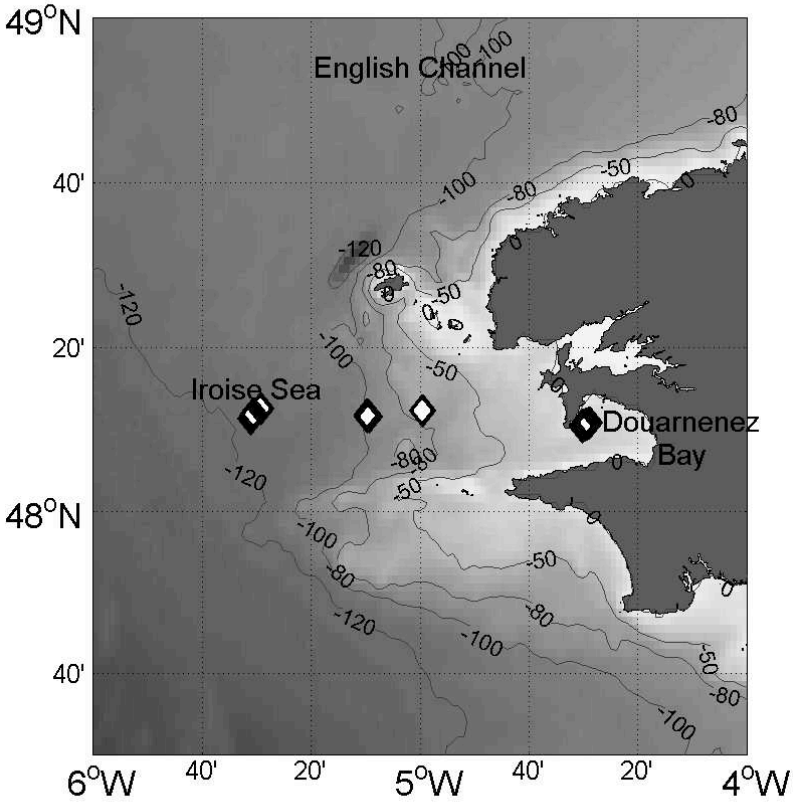

Figure 4. Locations from which OCARINA was operated during the FROMVAR 2011 experiment. The bathymetry is indicated with contour lines.

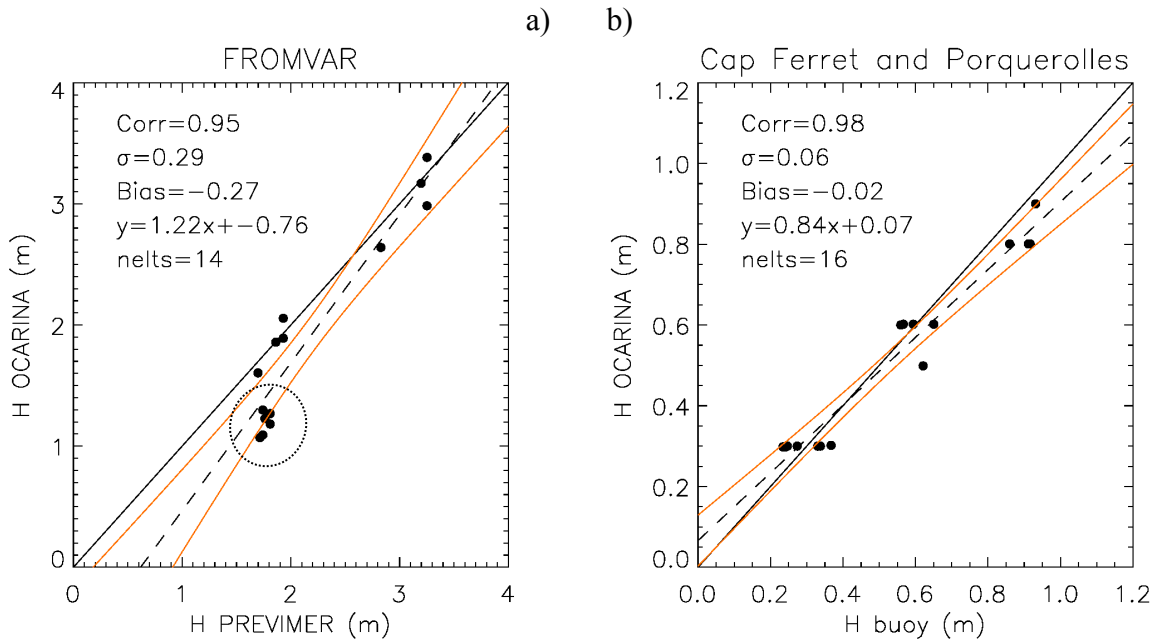

Figure 5. Comparison between [illegible] from PREVIMER model versus OCARINA estimates (panel a). The dashed lines indicate the linear fits between [illegible] estimates on the *x* and *y* axes. The red lines indicate the 95% confidence interval for the linear fit. The dots in the black circle correspond to data taken in shallow water. In panel b, the estimates of [illegible] were compared to reference wave buoy data, near Porquerolles and Cap Ferret, which were collected during the first tests of OCARINA, in 2010. 'nelts'means 'number of elements/ cases'.

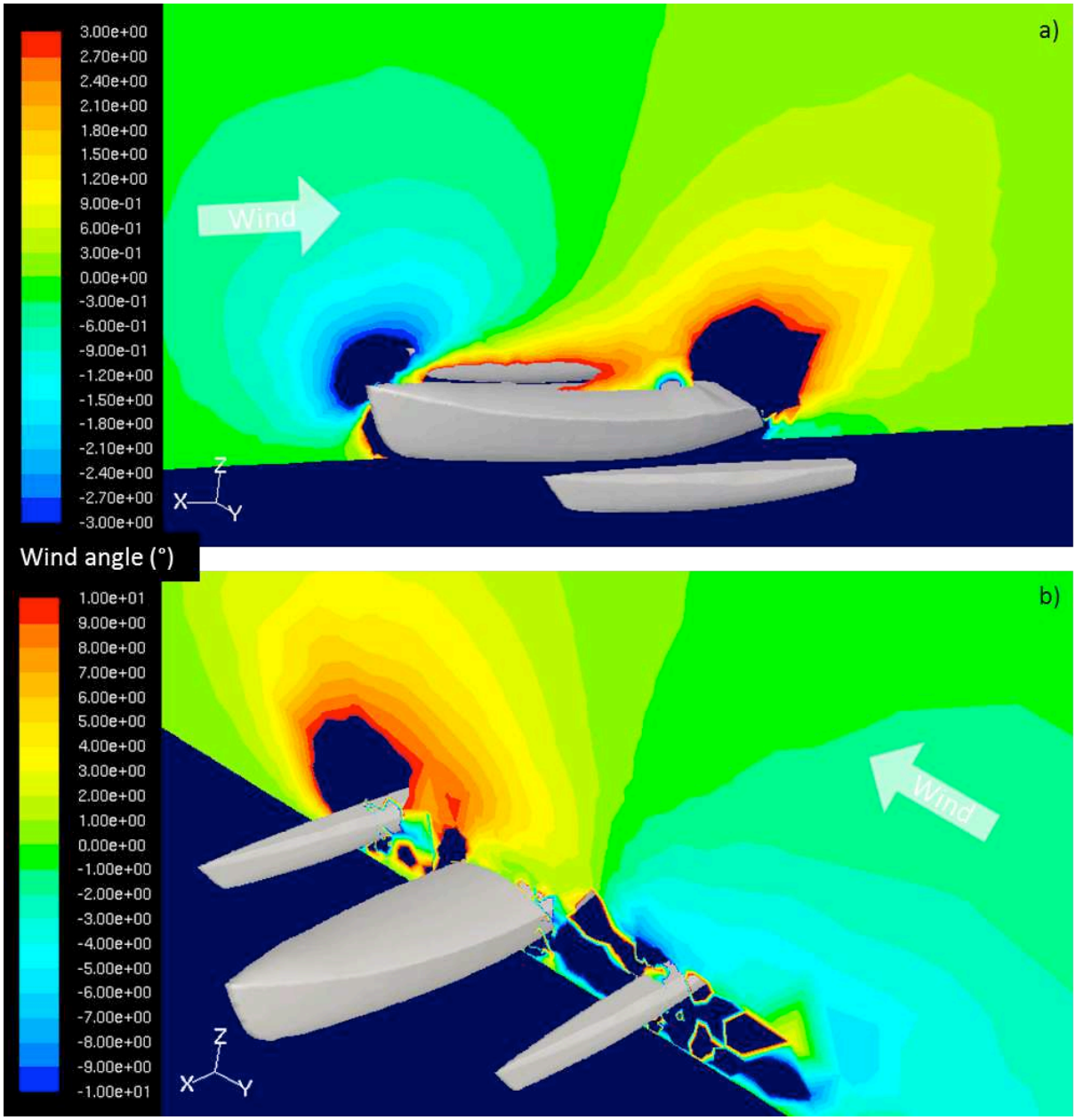

Figure 6. Numerical simulations of the vertical wind angle (in degrees), with the hypothesis that OCARINA is horizontal. In panel a, wind is aligned with the longitudinal axis of the boat, whereas the wind comes from the portside of the boat in panel b. Gaps in panels a, b correspond to regions where the absolute value of the angle is larger than three, ten degrees, respectively.

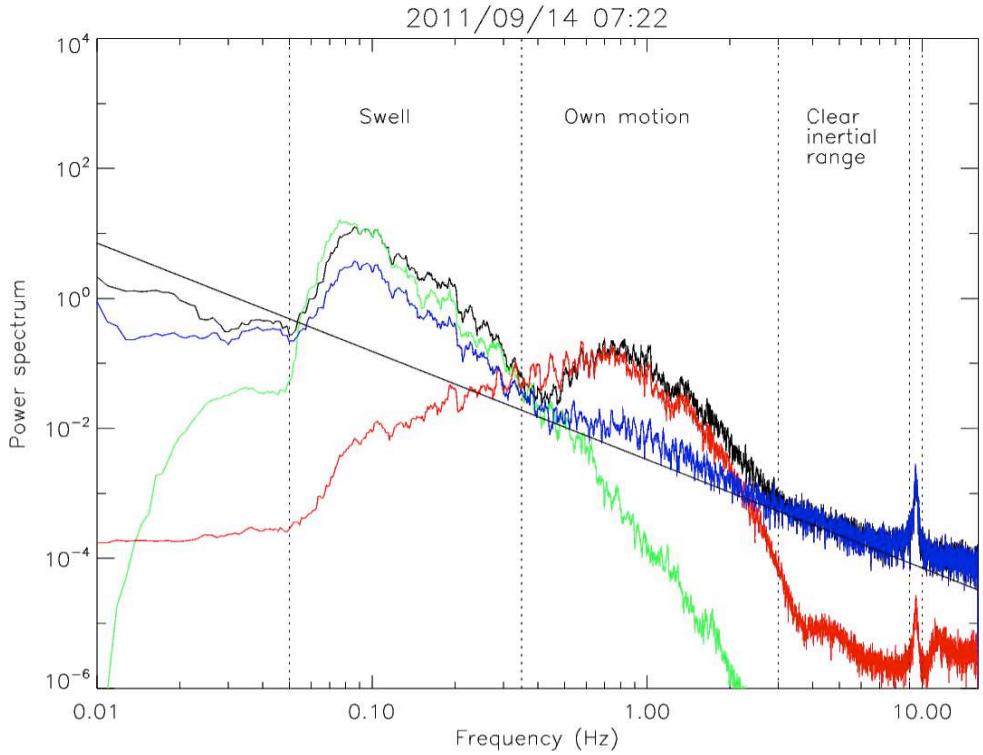

Figure 7. Non-corrected horizontal wind component (black), Sea elevation (green), Linear speed due to roll angle (red), and corrected horizontal wind component (blue). The oblique black line shows the -5/3 slope within the log/log axis.

a)

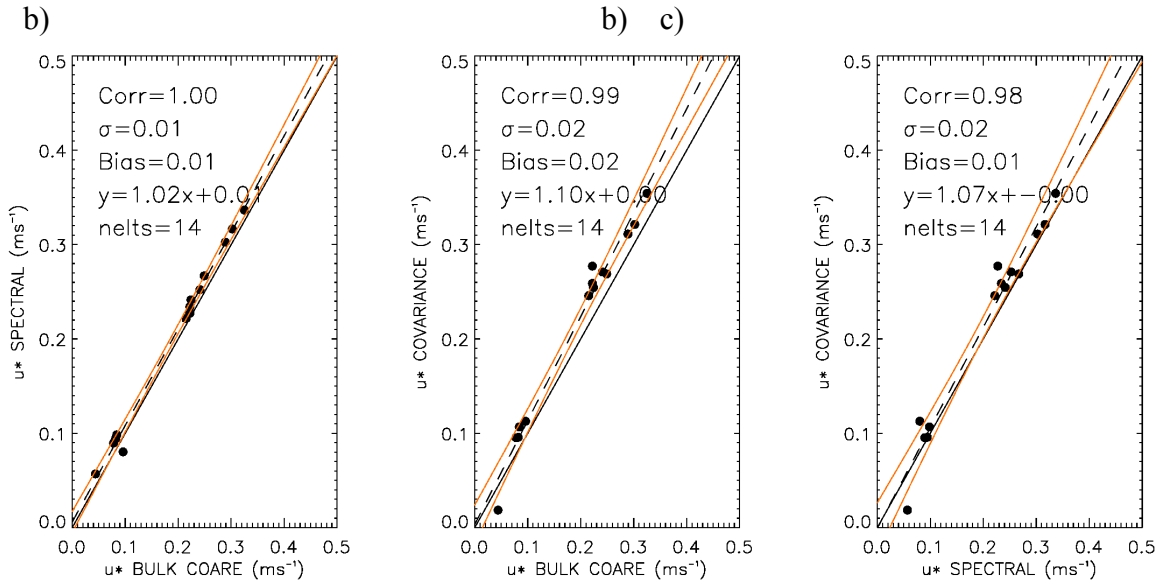

Figure 8. Comparison between *u** values calculated with three different methods: ID (also named SPECTRAL) versus bulk in panel a, EC (also named COVARIANCE) versus BULK in panel b and EC versus SPECTRAL in panel c). The red lines indicate the 95% confidence interval for the linear fit. The cut-off time period of the high pass filter was set to 1 000 sec for the EC method. 'nelts' means 'number of elements/cases'.

a)

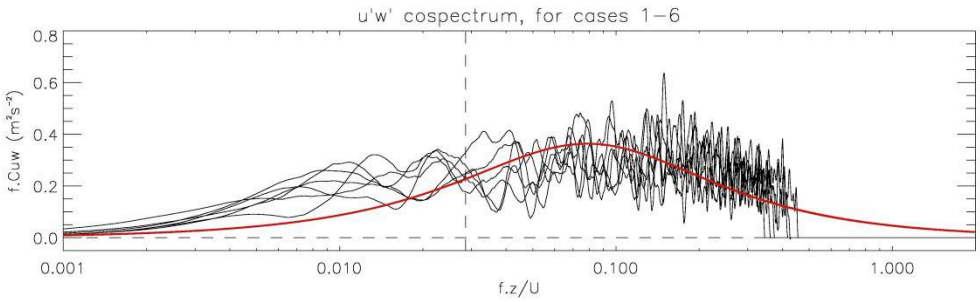
u'w' cospectrum, for cases 1−6
f.Cuw (m²s⁻²)
0.8
0.6
0.4
0.2
0.0
0.001
0.010
0.100
1.000
f.z/U

b)

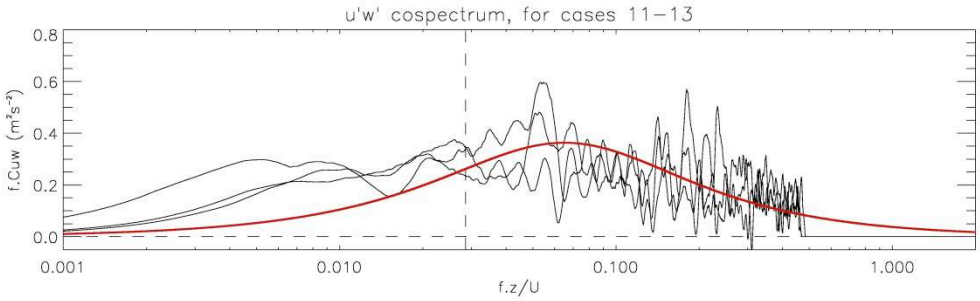
u'w' cospectrum, for cases 11−13
f.Cuw (m²s⁻²)
0.8
0.6
0.4
0.2
0.0
0.001
0.010
0.100
1.000
f.z/U

c)

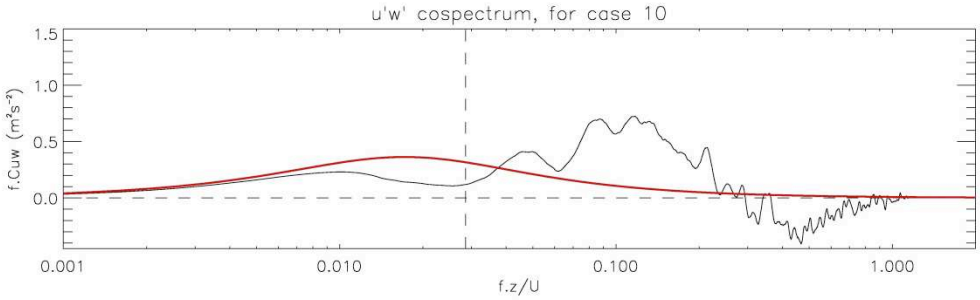
u'w' cospectrum, for case 10
f.Cuw (m²s⁻²)
1.5
1.0
0.5
0.0
0.001
0.010
0.100
1.000
f.z/U

d)

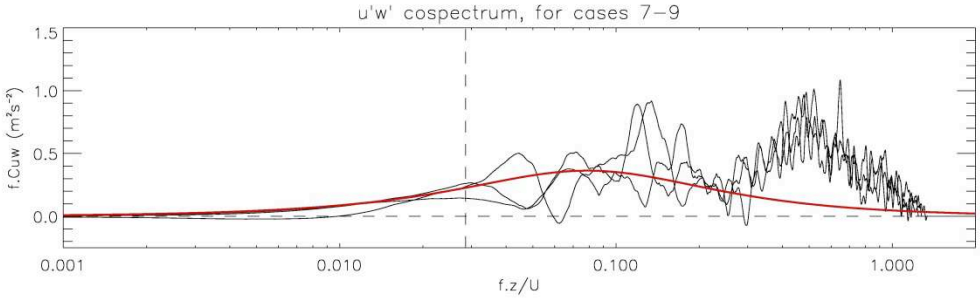
u'w' cospectrum, for cases 7−9
f.Cuw (m²s⁻²)
1.5
1.0
0.5
0.0
0.001
0.010
0.100
1.000
f.z/U

e)

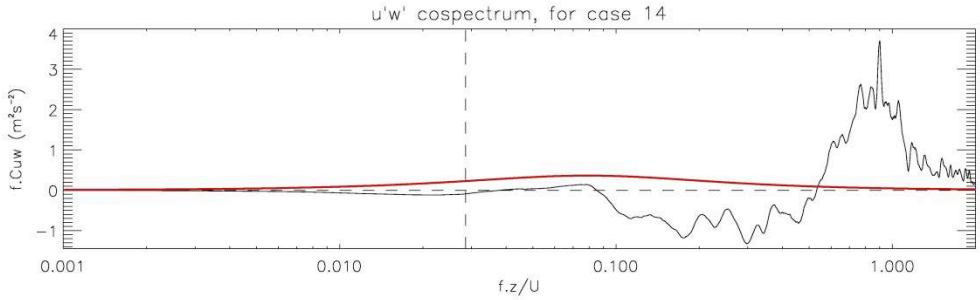
u'w' cospectrum, for case 14
f.Cuw (m²s⁻²)
4
3
2
1
0
−1
0.001
0.010
0.100
1.000
f.z/U

Figure 9. Cospectra of u'w' for the fourteen cases. Cases that presented a similar behaviour were grouped. The red line represents the empirical model of Kaimal et al. (1972).

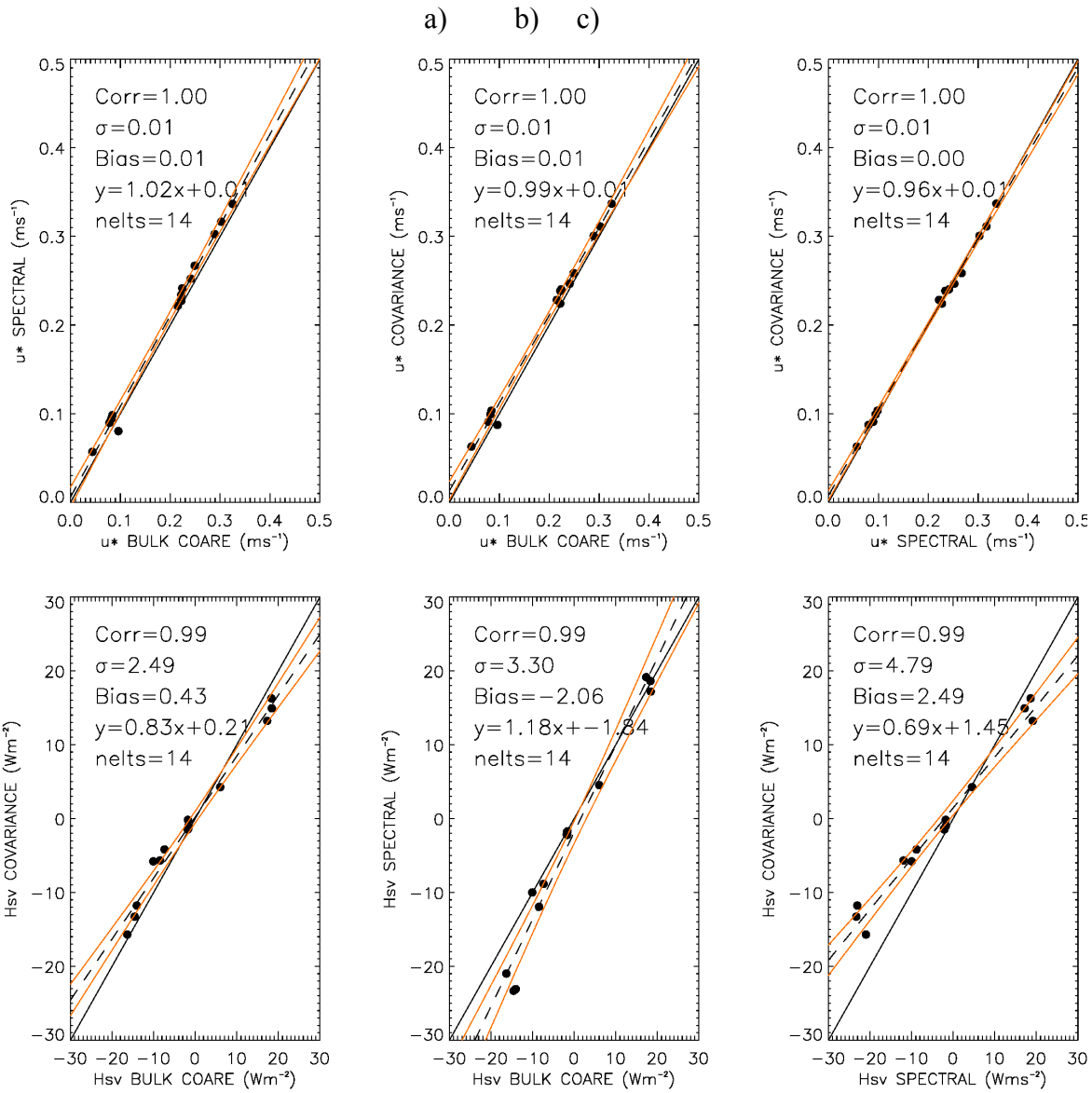

Figure 10. Comparison between friction velocity (*u**) and buoyancy flux (*Hsv*) estimates, with three different methods (EC, ID and bulk). The red lines indicate the 95% confidence interval for the linear fit. The cut-off time period of the high pass filter was set to 35 sec for application of the EC method.

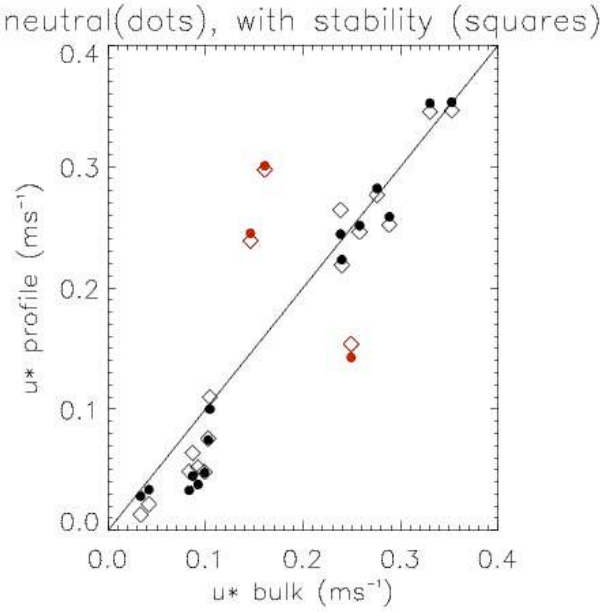

Figure 11. Comparison of $u*$ values estimated with the profile method and with the bulk method. The red marks correspond to situations when the wind came from the starboard side of OCARINA, for which there may be an aerodynamic masking effect because of the starboard mast and the central mast. The empty diamonds correspond to calculations that account for stability, whereas the dots correspond to a neutral surface boundary layer hypothesis.

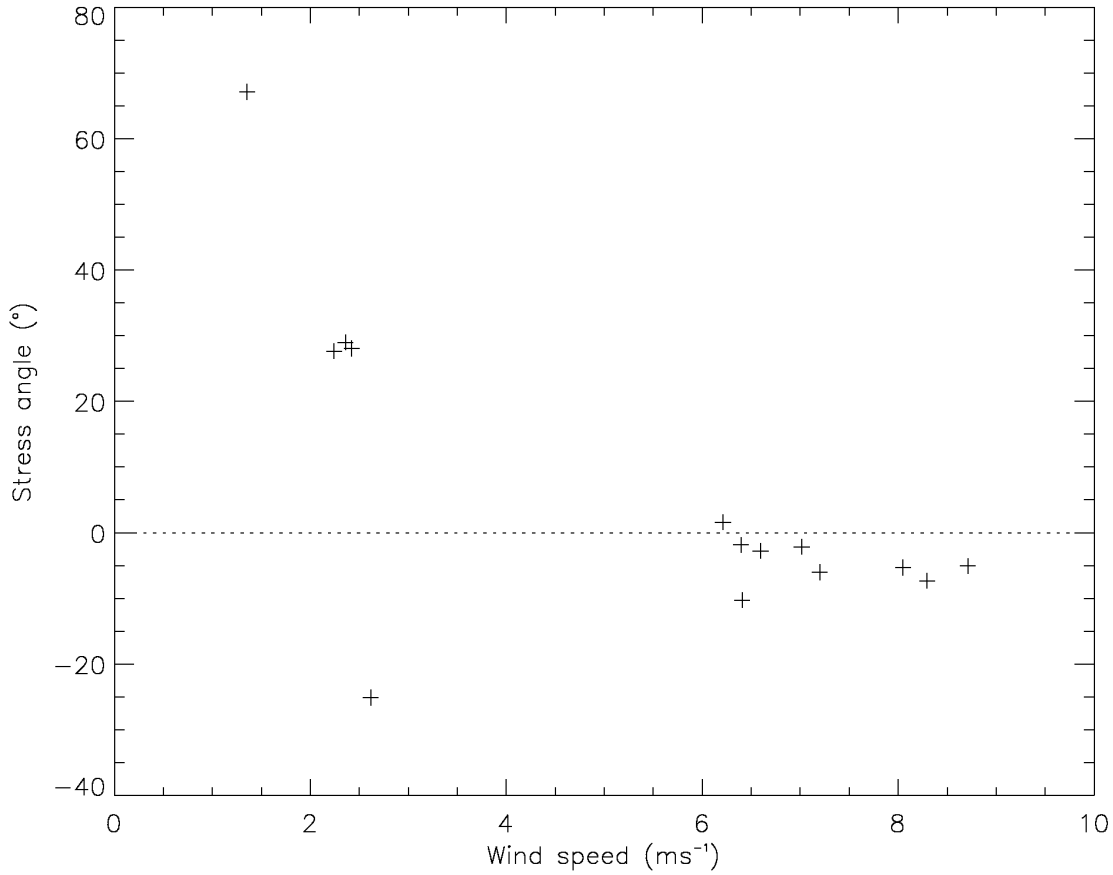

Figure 12. Angle between the turbulent stress and the along wind mean direction, as a function of the true wind speed.

a)

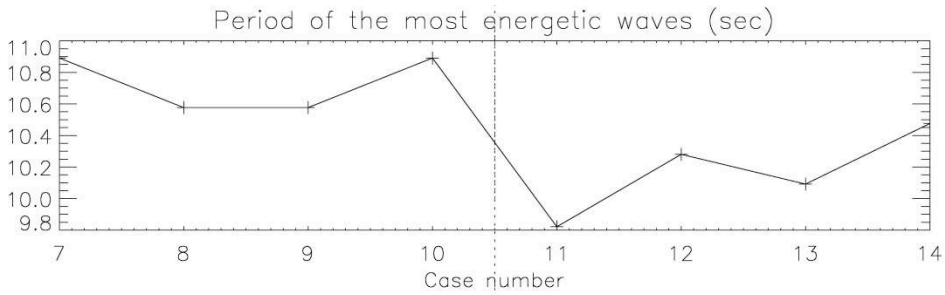
Period of the most energetic waves (sec)
11.0
10.8
10.6
10.4
10.2
10.0
9.8
7
8
9
10
11
12
13
14
Case number

b)

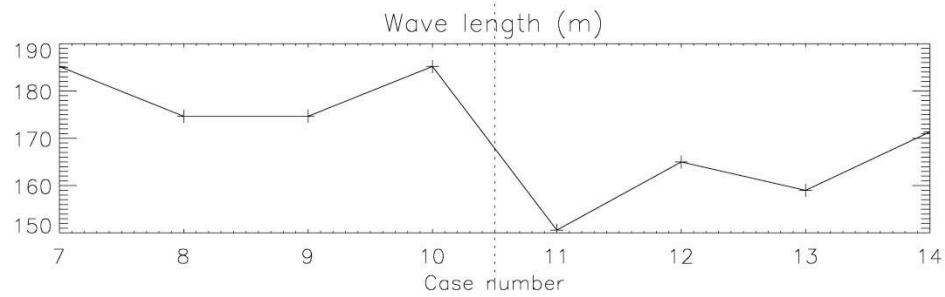
Wave length (m)
190
180
170
160
150
7
8
9
10
11
12
13
14
Case number

c)

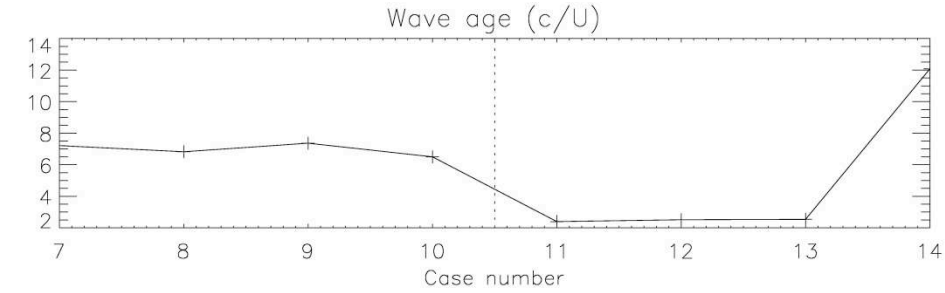
Wave age (c/U)
14
12
10
8
6
4
2
7
8
9
10
11
12
13
14
Case number

d)

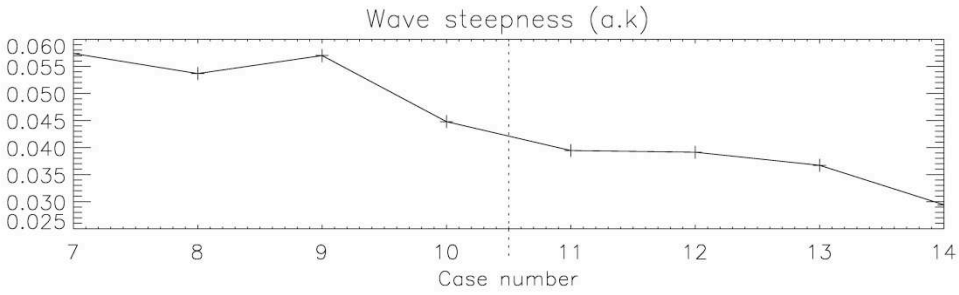
Wave steepness (a.k)
0.060
0.055
0.050
0.045
0.040
0.035
0.030
0.025
7
8
9
10
11
12
13
14
Case number

e)

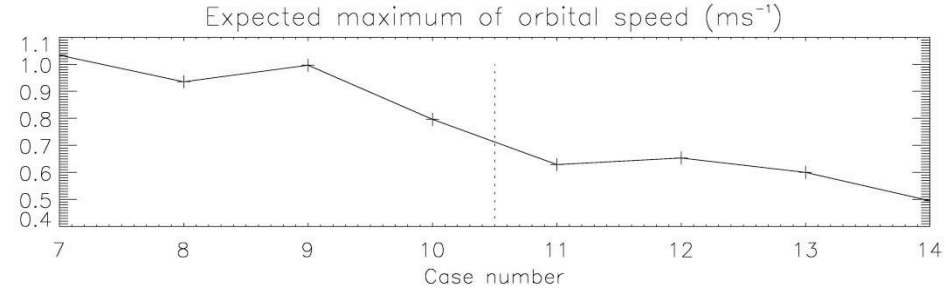
Expected maximum of orbital speed (ms⁻¹)
1.1
1.0
0.9
0.8
0.7
0.6
0.5
0.4
7
8
9
10
11
12
13
14
Case number

Figure 13. Wave characteristics in open ocean conditions, during the FROMVAR experiment. On the *x*-axis, one graduation corresponds to one 20-min bin. In panels c,d, both wave age and wave steepness are dimensionless quantities.

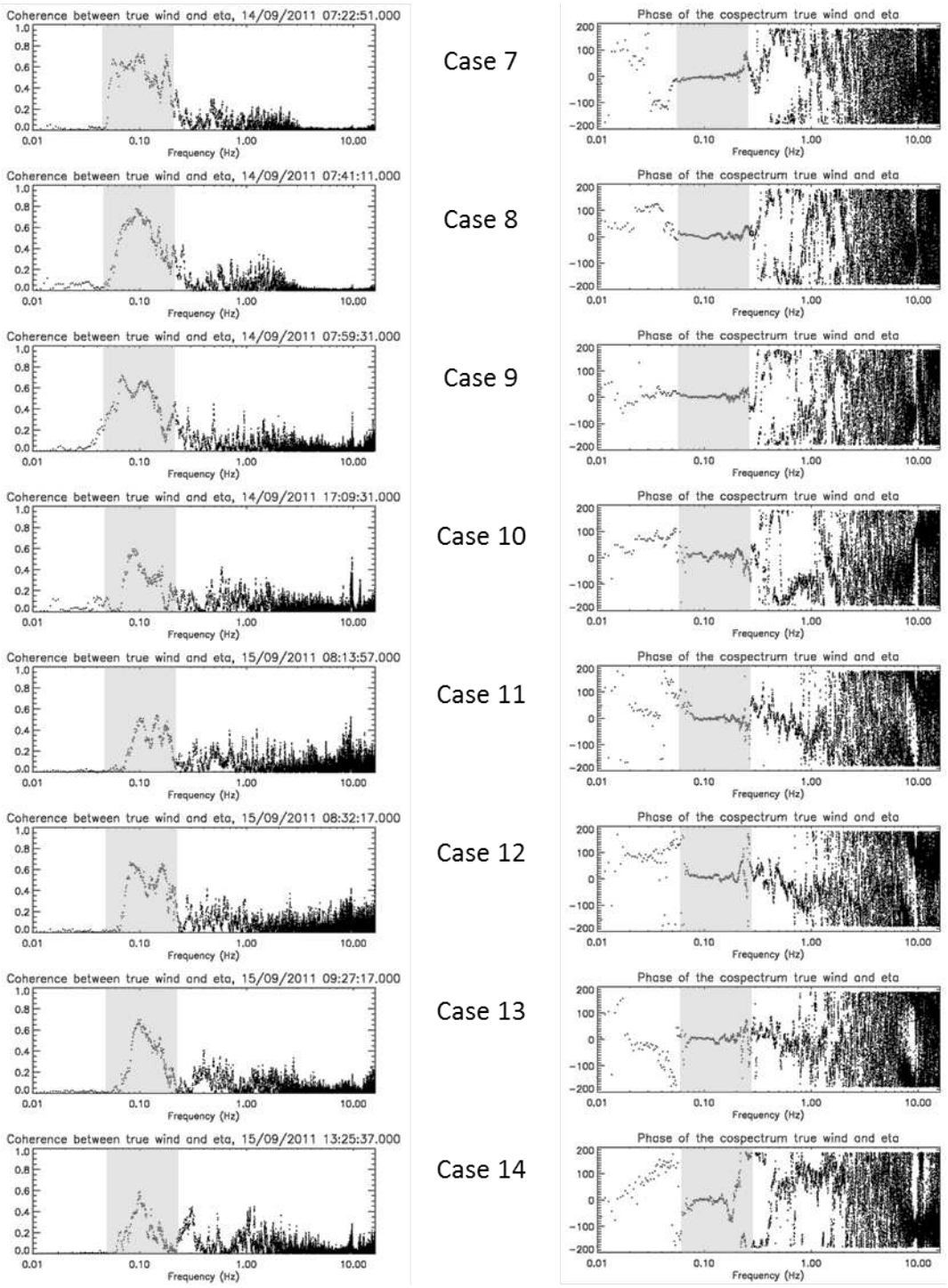

Figure 14. Spectra of coherence (left panels) and phase (right panels) between wind and sea surface elevation (eta). The greyed areas highlight the spectral regions of the swell, where the coherence is the largest. Phases are expressed in degrees. Each spectrum is calculated on a 20-min interval that starts at the time indicated in the panel title.

a)

b)

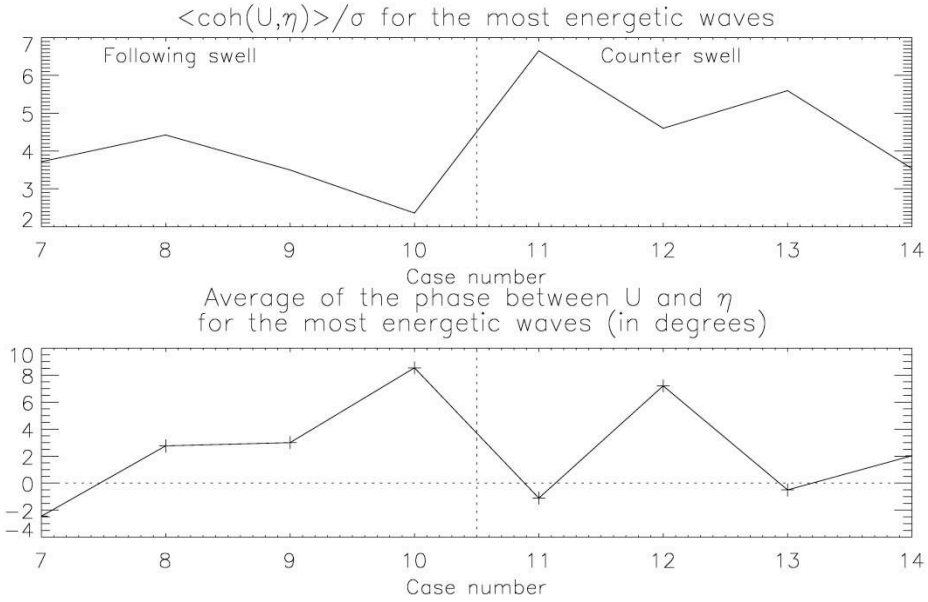

Figure 15. Detection of coherence between U and [illegible], for the spectral region of the swell (in panel a), and phase between U and [illegible] (panel b). In panel a, the coherence between U and [illegible] is detected because the values are larger than two for all cases.